

## Mining of Potential Antifungal Molecules for Control of *Fusarium fujikuroi* in Rice using *in silico* and *in vitro* Analysis

Randeep Kumar<sup>1</sup>, Abhishek Mandal<sup>1,5\*</sup>, Aditi Kundu<sup>1</sup>, Bishnu Maya Bashyal<sup>2</sup>, Neeraj Patanjali<sup>1</sup>, Anirban Dutta<sup>1,4</sup>,  
Gopala Krishnan S<sup>3</sup>, A K Singh<sup>3</sup> & Anupama Singh<sup>1\*</sup>

<sup>1</sup>Division of Agricultural Chemicals, <sup>2</sup>Division of Plant Pathology, <sup>3</sup>Division of Genetics and Plant Breeding,  
ICAR-Indian Agricultural Research Institute, New Delhi 110 012, India

<sup>4</sup>Downstream Agro-Processing Division, ICAR-National Institute of Secondary Agriculture,  
Namkum, Ranchi 834 010, Jharkhand, India

<sup>5</sup>Division of Basic Sciences, ICAR-Indian Institute of Horticultural Research, Bangalore 560 089, Karnataka, India

Received 22 June 2023; revised 18 August 2023; accepted 09 September 2023

A library of 170 fungicidal molecules of different functional moieties were subjected to *in-silico* assessment of their relative potential to inhibit ten vital targets of the *Fusarium fujikuroi*, bakanae disease causative pathogen in rice. Targets chosen were tubulin proteins ( $\alpha$ -,  $\beta$ - and  $\gamma$ -tubulin) and NRPS31 gene cluster (FFUJ\_00005, FFUJ\_00006, FFUJ\_00007, FFUJ\_00008, FFUJ\_00010, FFUJ\_00011, FFUJ\_00013). *In-silico* findings were validated with the help of *in vitro* analysis of the molecules to predict the most effective compound(s) relative to carbendazim (positive control). Most effective molecules were selected based on their chemical characteristics and Lipinski's rule. One each of the natural and synthetic origin molecules was selected for the molecular dynamics and *in-vitro* analysis.  $\beta$ -Caryophyllene came out as the most potential molecule followed by flusilazole. The extent of inhibition of  $\alpha$ -tubulin by these two molecules was significantly higher than by carbendazim. *In-vitro* bioassay validated the *in-silico* findings with LC<sub>50</sub> values of 3.29, 64.12, and 178.77  $\mu$ g/mL for  $\beta$ -caryophyllene, flusilazole and carbendazim, respectively. Further, molecular dynamics also revealed the selected molecular complex as highly effective with time when analyzed using Root Mean Square Deviation (RMSD) and Radius of Gyration (R<sub>g</sub>).

**Keywords:** Carbendazim, Docking, Flusilazole, Molecular dynamics,  $\beta$ -Caryophyllene

### Introduction

*Fusarium fujikuroi*, a phytopathogenic fungus is known to cause "bakanae" disease or foolish seedling disease of rice. The fungus excessively produces gibberellic acid, which results in excessive vegetative growth and negligible reproductive growth of the plant. The severity of the disease is linked to the excessive production of gibberellic acid and toxins like fusarins, moniliformin, beauvericin and fumonisins.<sup>1</sup> Due to the produced empty grains in the infected plants, the disease is referred to as 'Foolish Seedling Disease'.<sup>2</sup> Globally, it has been estimated to result in almost 50% yield losses and therefore, the disease is one of a serious concern in rice growing regions of south-east Asia.<sup>3</sup> Researchers across the world are engaged in deciphering the mechanism and developing strategies to combat this disease.

Previous studies suggest some of the potential fungicides as effective against the disease. Li et al.<sup>4</sup> reported that ipconazole and phenamacril were highly effective in controlling the disease with the EC<sub>50</sub> values of 0.0472 g/mL and 0.1544 g/mL, respectively. These two molecules have been registered for use against bakanae disease in China and Japan.<sup>5</sup> Some studies also suggested the use of carbendazim for seed treatment @ 2.5 g/kg seed followed by foliar spray @ 2.5 g/L to manage the disease. There are however, prominent reports of confirmed issues regarding resistance development to carbendazim.<sup>6</sup>

Limited available options to manage bakanae disease, resistance issues, expanding severity of disease in newer regions further to Japan and China, warrant a systematic research endeavour to identify the potential lead molecules and the possible combinations of potential molecules from natural and synthetic origin. India does not have any registered product against bakanae disease so far. Hence, it becomes more relevant to conduct fungicidal product development

\*Authors for Correspondence  
E-mail: abhishekmandal.iari@gmail.com;  
anupamanil2000@gmail.com

related research in the stated context. Identification of new drug candidates requires an extensive investigation of drug ligand-target interactions *in-silico* as the first step. In structural molecular biology and computer-assisted drug creation, molecular docking is a crucial tool. Predicting the dominant binding mode(s) of a ligand with a protein having a known three-dimensional structure is the aim of ligand-protein docking. The binding affinity of the molecules towards the vital target proteins is assessed as a function of their significant biological activity. The drug discovery programs commonly target the micro tubular protein assembly disruption. It is essential for the development of new medications using such drug discovery programs is to take into account the growing understanding that microtubule dynamics play a fundamental role in cell proliferation and mitosis and inhibiting spindle microtubule dynamics may be sufficient to cause cell death.<sup>7</sup> Fungal Microtubules (MTs) are comprised of three subunit proteins namely  $\alpha$ -,  $\beta$ - and  $\gamma$ -tubulins which play a crucial role in vital cell functions like mitosis, and cytoplasmic transport.<sup>11</sup> Out of these three proteins,  $\gamma$ -tubulin acts as a template protein and regulates the nucleation of microtubular structure while the other two dimers polymerize to form microtubular structure.<sup>8</sup> Further, in context of bakanae pathogen, critical examination of the genes encoding biosynthesis of the secondary metabolites revealed several enzymes such as Non-Ribosomal Peptide Synthetases (NRPSs), Polyketide Synthases (PKSs), Terpene Cyclases (TCs) and Dimethyl Allyl Tryptophan Synthases (DMATSSs), as responsible for biosynthesis of characteristic mycotoxins in various *Fusarium* spp.<sup>9,10</sup> Amid all the genomic sequences examined, two gene clusters namely, NRPS31 were unique and specific to the concerned pathogen. NRPS31 gene cluster comprising of seven genomic sequences namely FFUJ\_00005, FFUJ\_00006, FFUJ\_00007, FFUJ\_00008, FFUJ\_00010, FFUJ\_00011 and FFUJ\_00013 plays a major role in gibberellic acid biosynthesis, and it is also involved in generation of apicidin like compounds, that act as Histone Deacetylase (HDACs) inhibitors.<sup>11,12</sup> Nevertheless, these seven gene sequences are also involved in biosynthesis of several major secondary metabolites responsible for regulation of vital enzymes (Table 1).<sup>13</sup> However, comprehensive investigation is still required in order to develop a suitable antifungal agent for the management of bakanae disease.

Novelty of the present research work lies in the fact that there is no fungicide registered for use against the

Table 1 — Seven genes of the NRPS31 gene cluster and the associated enzymes involved<sup>11</sup>

S.No.	Genes	Associated enzyme
1.	FFUJ_00005	Isoamyl alcohol oxidase
2.	FFUJ_00006	Cytochrome P-450
3.	FFUJ_00007	Benzoate para hydroxylase
4.	FFUJ_00008	<i>o</i> -Methyl transferase
5.	FFUJ_00010	Fatty acid synthase
6.	FFUJ_00011	Branched chain amino acid amionotransferase
7.	FFUJ_00013	PRO <sub>3</sub> $\delta$ -1-pyrroline-5-carboxylate reductase

disease across the world. And, also computational aided drug design program haven't been yet utilized fully for unraveling the interaction of pesticide molecules and target specific enzymes of plant pathogens. Furthermore, molecular dynamics and simulation has rarely been exploited for its potential use in fungicide development. Keeping in view, the research gaps were identified and efforts were being made to explain the interaction of various potential molecules with the specific gene cluster of the target pathogen. Herein, we report our finding of computational *in-silico* assessment of relative interaction of 170 fungicidal candidate molecules with NRPS31 gene cluster and tubulin binding sites with an aim to identify the most potential molecules that qualify for further product scale R&D.

## Materials and Methods

### Molecular Docking and Simulation

One hundred and seventy molecules were selected based on comprehensive review of the literature reports citing their fungicidal action against phytopathogenic fungi and all the fungicides registered so far. Molecular docking was performed against ten major target proteins of *F. fujikuroi*.

### Selection of Proteins

Two gene complexes comprising ten target proteins namely tubulin proteins ( $\alpha$ -,  $\beta$ -, and  $\gamma$ -tubulin) and NRPS31 gene cluster proteins (FFUJ\_00005, FFUJ\_00006, FFUJ\_00007, FFUJ\_00008, FFUJ\_00010, FFUJ\_00011 and FFUJ\_00013) were selected as vital target receptors proteins for the *in-silico* screening. Tubulin proteins namely,  $\alpha$ -,  $\beta$ -, and  $\gamma$ -tubulin associated in the structural and functional organization of the microtubules;  $\alpha$ - and  $\beta$ -tubulin polymerize to maintain structural integrity of microtubules while,  $\gamma$ -tubulin helps in the nucleation of the microtubular assembly and maintains its polarity.<sup>9</sup> NRPS31 gene cluster is related to functioning of vital enzymes such as isoamyl alcohol

oxidase, cytochrome P450, benzoate para hydroxylase, *O*-methyl transferase, fatty acid synthase, branched chain amino acid amino-transferase, and delta-1-pyrroline-5-carboxylate reductase, respectively.<sup>11</sup>

#### **Preparation of 3-D Structure of Receptor Protein**

The amino acid sequences of the tested target proteins were obtained from NCBI database (NCBI, 2023). Furthermore, templates suitable for constructing the secondary structures of the chosen amino acid sequences were found using the NCBI blast tool and PDB database. Thereafter, Modeller v 9.24 was used to model homology protein structures and saved in .pdb format.<sup>14,15</sup> To verify the accuracy of the modeled receptor protein, the quality was assessed through PROCHECK software.<sup>16</sup>

#### **Ligand Preparation**

The 3-D molecular structures of the fungicidal compounds used for the molecular docking are implied by the term "ligands" in the context of the current investigation. PUBCHEM database<sup>3</sup> and Chem Draw Ultra 11.0 software were used to obtain the 3-D structures of the all the molecules to be screened and were saved in .sdf format. Five parameters related to determination of fungicidal likeness namely drug-likeness score (DLS), water/lipid coefficient (LogP), Number of Hydrogen Bond Donor (NHBD), Number of Hydrogen Bond Acceptor (NHBA) and Molecular Weight (MW) was obtained using MolSoft (New MolSoft ICM 3.8-3) software.<sup>17</sup>

#### **Molecular Docking**

Using the software See SAR v10.3.1, in-silico molecular docking simulation investigations were carried out. The vacant active site residues were found and the receptor protein structure was created using homology modelling. Both 3-D and 2-D frameworks were created for the whole set of molecules. After docking, the binding affinity was calculated using Hydrogen DEhydration (HYDE) scoring, which depends on the octanol-water partition coefficients (Kow) of small molecules and is based on the desolvation and hydration processes. The ligands' estimated affinities for binding to the receptor proteins ranged from mM to pM. To identify the best configurations, additional factors including torsion quality, clashes, Ligand Efficiency (LE), and Lipophilic Ligand Efficiency (LLE) were also taken into account.<sup>18</sup>

Additionally, flexible ligand docking was performed utilising the ICM software, which optimizes the internal coordinates of the ligand molecules within the grid

potential maps through the use of Monte Carlo simulations. Using Discovery Studio v4.1, the interactions between the docked receptor and ligands were examined.<sup>14,15</sup>

#### **Molecular Dynamics**

Using the parameterization included in Discovery Studio 4.1 and the CHARMM force field, MD simulations of the apo-protein and protein complexes were performed. An explicit solvation model with pre-equilibrated TIP3P water molecules was used for the simulations. The protein complexes were arranged in a truncated octahedral box, with at least 10 separating any two atoms of the -tubulin: ligand complex from the box faces. With the exception of the apo-protein/complex, the water box contained 943 water molecules together with 3 Na<sup>+</sup> and 3 Cl<sup>-</sup> ions to create a counter ion concentration of 0.145 M. The simulation was run twice, first by minimizing the complex's shape while holding the protein and its ligand constant and just allowing the water molecules to move in different directions. A complete system minimization came next. Then, using a time step of 2 fs, a heating phase of 100 ps, an initial temperature of 50 K, and a goal temperature of 300 K, an MD simulation was run. Then, equilibration was performed under periodic boundary conditions while maintaining a constant volume and temperature. The temperature was then maintained at 303.15 K using Langevin dynamics with a collision frequency of 1.0 ps<sup>-1</sup> during a production run of 30 ns MD simulation in the NPT ensemble.

The simulations were run using the Standard Dynamics Cascade module, and the hydrogen atom bond lengths were restricted using the SHAKE method. The Verlet leapfrog technique was used to integrate the equations of motion, using a time step of 2 fs. In order to account for long-range interactions, the Particle-Mesh Ewald (PME) approach was used, and a non-bonded interaction limit of 10 was used. The Analyze Trajectory module of Discovery Studio 4.1 was used to examine the 300 conformations that resulted from saving the MD trajectory every 2 ps. The electrostatic contribution to the solvation energy was calculated using the two-step Solvation Energy methodology and the DelPhi programme.<sup>19</sup>

#### **In-vitro Fungicidal Bioassay**

##### **Chemicals and Reagents**

All solvents used in the bioassay experiment were of analytical reagent (AR) grade and were purchased from Merck®. The powdered formulation of Potato

Dextrose Agar (PDA) was obtained from Himedia Laboratories Pvt. Ltd. The compound  $\beta$ -Caryophyllene was procured from TCI (C0796), and flusilazole with a purity of 98.75% was obtained from UPL Ltd.

#### Fungal Culture

Fungal culture of *F. fujikuroi* Nirenberg isolate F-309 was collected from ITCC (Indian Type Culture Collection), ICAR-Indian Agricultural Research Institute (ICAR-IARI), New Delhi, India and the culture was maintained by sub-culturing on PDA media and kept for growing at  $27 \pm 1^\circ\text{C}$  incubation temperature in BOD.

#### Poisoned Food Assay

Best screened individual molecules of natural and synthetic origin,  $\beta$ -caryophyllene and flusilazole were assessed for antifungal activity against *F. fujikuroi* strain F-309 using poisoned food technique, slightly modified by the process suggested by Dutta *et al.*<sup>15</sup> To prepare the Potato Dextrose Agar (PDA) media, 39 g of PDA powder was dissolved in 1 L of distilled water. The media was then sterilized using an autoclave at  $120^\circ\text{C}$  for 30 minutes. Stock solutions of the tested compounds,  $\beta$ -caryophyllene (0.01 g) and flusilazole (0.05 g) were separately dissolved in 2 mL of dimethyl sulfoxide (DMSO). These stock solutions were further diluted with the media to obtain the desired test concentrations: 100–6.25  $\mu\text{g/mL}$  for  $\beta$ -caryophyllene and 500–31.25  $\mu\text{g/mL}$  for flusilazole.

Various treatment concentrations of the prepared media were put into sterilised petri plates and given time to harden. Using a cork borer, 10 mm-diameter mycelial discs were extracted from a 10-day-old fungal culture and positioned in the middle of each petri dish. Plates devoid of any chemicals were infected as negative controls in addition to the treated plates. As a positive control, bavistin (Carbendazim 50WP; BASF India Ltd.) was utilised at doses ranging from 500 to 31.25 g/mL. The petri plates were incubated in a BOD incubator at  $27^\circ\text{C}$  with three replicates maintained for each treatment. A measurement of the mycelial growth was made after 10 days of incubation. Using the following formula, the percentage of mycelial growth inhibition was determined:

$$\text{Inhibition of growth (\%)} = (C - T/C) \times 100$$

where, D is the typical size of the mycelial growth in the treated plates, whereas C is the typical size of the mycelial growth in the replicates used as controls.

#### Statistical Analysis

Software from SPSS (Version 14.0, IBM Corp., Armonk, NY, USA) was used to analyse the data. A one-way Analysis Of Variance (ANOVA) was carried out to determine the importance of variance between various variables. In order to ascertain the statistical significance of the tests, the significance threshold was set at 5% ( $p < 0.05$ ). Polo Plus software was used to carry out a probit analysis on the % inhibition data. Using this study, the lethal concentrations (LC50), which are given in g/mL, were determined.

#### Results and Discussion

Initially a total of 170 molecules of different fungicidal moieties were screened against 10 vital target proteins of *F. fujikuroi* using molecular docking and dynamics. Based on the performance in molecular docking and simulation studies, the best five molecules for each target protein were selected and represented in Table 2. Finally, the two most efficient molecules, one each from the natural and synthetic origin,  $\beta$ -caryophyllene and flusilazole were selected for molecular dynamics studies and validated through *in-vitro* antifungal assessment against *F. fujikuroi*.

#### Screening for Binding Affinity

In the case of  $\alpha$ -tubulin, the top five molecules exhibited way greater affinity than that of the commercially used fungicides (carbendazim, ipconazole, and phenamacril). The order of binding affinity is as follows: Monolaurin > Plaunotol > Caryophyllene > Penconazole > Flusilazole > Ipconazole > Phenamacril > Carbendazim. Similarly, in the case of  $\beta$ -tubulin the order was as follows: Bisabolene > Crassinervic acid > Ametoctradin > Plaunotol > Dodine > Carbendazim > Ipconazole > Phenamacril. Also, when screened against  $\gamma$ -tubulin the binding affinity follows the order Monolaurin > Flusilazole > Metalaxyl > Citronellol > Gramine > Phenamacril > Ipconazole > Carbendazim (Table 2).

Similarly, screening was also conducted for binding affinity against the NRPS31 gene cluster (Table 2) and the top five molecules were found to possess significantly higher binding affinity than those of the commercially utilized fungicides. In the first target gene, FFUJ\_00005, the binding affinity follows the order of Linolenic acid > Monocaprin > Monolaurin > Thymol > *p*-Cymene > Ipconazole > Carbendazim > Phenamacril. A similar case is with the second gene,

Table 2 — *In-silico* antifungal activity of all the putative fungicidal moieties selected after screening against 10 vital target proteins of *F. fujikuroi*

Target proteins	Identified compounds	M.wt	LogP	Binding affinity range (nM)	ΔG	LE	LLE
α-tubulin	Monolaurin	274.39	2.80	0.019 < KI < 1.91	-55.4	++	++
	Plaunotol	306.48	5.09	0.13 < KI < 13.4	-50.6	++	0
	Penconazole	284.18	4.16	40.04 < KI < 3978.24	-36.6	+	-
	Flusilazole	315.39	2.25	69.40 < KI < 6896.25	-35.5	+	0
	Caryophyllene	204.35	4.72	16.05 < KI < 1595.40	-40.5	++	-
	Ipconazole	333.86	3.58	15583.521304 < KI < 1548314.978629	-21.7	---	-
	Phenamacril	216.23	1.44	6791598.505353 < KI < 674785466.61513	-6.8	---	---
	Carbendazim	191.18	1.74	7800565.458354 < KI < 775032298.880517	-6.2	---	---
β-tubulin	Bisabolene	204.35	5.17	78.98 < KI < 7848.04	-34.8	++	---
	Crassinervic acid	305.34	1.82	155.39 < KI < 15439.60	-31.6	0	0
	Ametoctradin	275.39	3.17	610.63 < KI < 60670.11	-29.6	0	-
	Plaunotol	306.48	5.09	1055.12 < KI < 104833.00	-28.3	0	---
	Dodine	228.40	1.26	4001.22 < KI < 397545.19	-25.5	-	0
	Ipconazole	333.86	3.58	176636505.704498 < KI < 17549881199.4153	6.5	---	---
	Phenamacril	216.23	1.44	70282002646.8761 < KI < 6982932503053.11	14.1	---	---
	Carbendazim	191.18	1.74	16554951964.3585 < KI < 1644832358281.42	11.8	---	---
γ-tubulin	Flusilazole	315.39	2.25	342.85 < KI < 34065.16	-31.1	0	-
	Gramine	175.25	0.81	6088.15 < KI < 604894.66	-24.0	+	-
	Metalaxyl	279.33	1.84	386.91 < KI < 38441.86	-30.8	0	0
	Monolaurin	274.39	2.80	112.35 < KI < 11163.49	-30.0	+	-
	Citronellol	156.26	2.75	1448.66 < KI < 143933.49	-27.7	++	-
	Ipconazole	333.86	3.58	8087328.865719 < KI < 803523938.881635	-5.5	---	---
	Phenamacril	216.23	1.44	4615118.74523 < KI < 458539334.080126	-7.7	---	---
	Carbendazim	191.18	1.74	104146115.999847 < KI < 10347532385.1546	0.2	---	---
FFUJ_00005	Thymol	150.21	2.82	17428.85 < KI < 1731659.48	-21.4	+	---
	<i>p</i> -cymene	134.22	3.11	34947.12 < KI < 3472203.55	-19.9	+	---
	Monocaprin	246.34	2.02	10293.79 < KI < 1022749.45	-22.8	0	---
	Linolenic acid	277.42	4.32	0.03 < KI < 3.41	-54.2	++	+
	Monolaurin	274.39	2.80	14186.53 < KI < 1409515.96	-22.0	-	---
	Ipconazole	333.86	3.58	133431965125527 < KI < 13257254647434300	35.1	---	---
	Phenamacril	216.23	1.44	350170721067.108 < KI < 34791531511171.9	20.3	---	---
	Carbendazim	191.18	1.74	27336735183759.1 < KI < 2716066268076270	31.0	---	---
FFUJ_00006	Plaunotol	306.48	5.09	0.015 < KI < 1.56	-56.0	++	0
	Nerolidol	222.36	4.39	0.08 < KI < 8.81	-51.8	++	0
	Oleic acid	281.45	4.77	0.06 < KI < 6.74	-55.0	++	0
	Phytol	296.53	6.36	0.00 < KI < 0.35	-59.6	++	0
	Linolenic acid	277.42	4.32	0.07 < KI < 7.07	-51.9	++	0
	Ipconazole	333.86	3.58	525087434.562684 < KI < 52170541186.4146	-4.0	---	---
	Phenamacril	216.23	1.44	676733.18095 < KI < 67237442.690568	-12.4	---	---
	Carbendazim	191.18	1.74	75354150.727034 < KI < 7486880403.72957	-0.6	---	---
FFUJ_00007	Folicanthine	376.54	0.251	46.97 < KI < 4667.10	-52.7	0	+
	10-hydroxy- <i>cis</i> -12-octadecenoic acid	297.45	3.74	9.39 < KI < 933.25	-40.0	+	0
	Plaunotol	306.48	5.09	14.83 < KI < 1473.63	-38.9	+	---
	Phytol	296.53	6.36	15.45 < KI < 1535.17	-39.1	+	---
	Oleic acid	281.45	4.77	25.02 < KI < 2486.01	-37.6	+	---
	Ipconazole	333.86	3.58	235205.99212 < KI < 23369105.96503	-15.0	---	---
	Phenamacril	216.23	1.44	42323.41808 < KI < 4205081.822074	-19.4	---	-
	Carbendazim	191.18	1.74	1267466.187722 < KI < 125930259.603402	-10.8	---	---

(Contd.)

Table 2 — *In-silico* antifungal activity of all the putative fungicidal moieties selected after screening against 10 vital target proteins of *F. fujikuroi*

Target proteins	Identified compounds	M.wt	LogP	Binding affinity range (nM)	ΔG	LE	LLE	
FFUJ_00008	Kitazin	260.29	4.10	45.19 < KI < 4490.26	-36.6	++	-	
	Undecylenic acid	183.26	2.04	20.26 < KI < 2013.25	-38.2	++	0	
	Propineb	224.39	0.21	570.96 < KI < 56728.63	-29.9	++	+	
	Plaunotol	306.48	5.09	0.01 < KI < 1.43	-59.1	++	0	
	Phytol	296.53	6.36	0.01 < KI < 1.49	-56.1	++	-	
	Ipconazole	333.86	3.58	319.120831 < KI < 31706.541316	-36.5	--	0	
	Phenamacril	216.23	1.44	8452054.260157 < KI < 839761563.246267	-6.1	--	--	
	Carbendazim	191.18	1.74	67559.179013 < KI < 6712403.876392	-18.2	--	0	
	FFUJ_00010	Terpinene	136.23	3.30	84.63 < KI < 8408.80	-34.7	++	-
		Citronellol	156.26	2.75	650.40 < KI < 64622.01	-29.6	++	-
Aduncumene		248.27	2.63	22.56 < KI < 2242.29	-38.1	++	0	
Plaunotol		306.48	5.09	332.95 < KI < 33081.22	-31.4	--	0	
10-hydroxy- <i>cis</i> -12-octadecenoic acid		297.45	3.74	0.86 < KI < 86.27	-46.0	++	0	
Ipconazole		333.86	3.58	4343260.097314 < KI < 431528570.054143	-15.9	--	--	
Phenamacril		216.23	1.44	1591023.770441 < KI < 158077618.470321	-11.1	--	-	
Carbendazim		191.18	1.74	5623619.761762 < KI < 558739872.802533	-7.1	--	--	
FFUJ_00011		Gramine	175.25	0.81	5693.53 < KI < 565686.55	-24.1	+	-
		Thiram	240.43	2.06	8611.37 < KI < 855591.30	-23.3	+	0
	Nerolidol	222.36	4.39	1007.48 < KI < 100099.53	-28.8	+	--	
	Calycanthine	348.49	0.20	34978.69 < KI < 3475340.47	-19.6	--	-	
	Monolaurin	274.39	2.80	4080.08 < KI < 405380.73	-25.1	0	--	
	Ipconazole	333.86	3.58	150316610.372728 < KI < 14934843982.6672	-0.1	--	--	
	Phenamacril	216.23	1.44	1091642313.14836 < KI < 108461118111.446	-3.6	--	-	
	Carbendazim	191.18	1.74	633757063.823555 < KI < 62967511359.1789	-3.5	--	--	
	FFUJ_00013	Geraniol	154.25	2.67	234.49 < KI < 23298.82	-32.1	++	-
		Thujone	152.23	2.25	1574.15 < KI < 156401.87	-27.4	++	-
Bisabolene		204.35	5.17	1728.54 < KI < 171741.20	-27.2	+	--	
Citronellol		156.26	2.75	2100.17 < KI < 208664.56	-26.8	++	--	
Monocaprin		246.34	2.02	2428.10 < KI < 241246.58	-39.0	0	-	
Ipconazole		333.86	3.58	2447494585.6094 < KI < 243173057813.515	-16.6	--	--	
Phenamacril		216.23	1.44	2103330801.46479 < KI < 208978351001.415	7.7	--	-	
Carbendazim		191.18	1.74	17719275126.4993 < KI < 1760514748463.45	3.2	--	--	

FFUJ\_00006, where, the binding affinity is in the order of Phytol > Plaunotol > Oleic acid > Linolenic acid > Nerolidol > Phenamacril > Ipconazole > Carbendazim. Likewise, in FFUJ\_00007, the molecular binding affinity follows the order 10-Hydroxy-*cis*-12-octadecenoic acid > Plaunotol > Phytol > Oleic acid > Folicanthine > Phenamacril > Ipconazole > Carbendazim. Similarly, in FFUJ\_00008, the binding affinity follows the order of Plaunotol > Phytol > Undecylenic acid > Kitazin > Ipconazole > Propineb > Carbendazim > Phenamacril. While, for FFUJ\_00010, the binding affinity range follows the order of: 10-Hydroxy-*cis*-12-octadecenoic acid > Aduncumene > Terpinene > Plaunotol > Citronellol > Phenamacril > Ipconazole > Carbendazim. A similar phenomenon is also observed in case of FFUJ\_00011,

where the binding affinity follows the order of Nerolidol > Monolaurin > Gramine > Thiram > Calycanthine > Phenamacril > Ipconazole > Carbendazim. Finally, for FFUJ\_00013 the order of binding affinity displayed as Geraniol > Thujone > Bisabolene > Citronellol > Monocaprin > Carbendazim > Phenamacril > Ipconazole.

#### Performance Based on Binding Energy

In the case of  $\alpha$ -tubulin, the top five molecules were observed to possess very high binding energy than that of the commercially used fungicides. The order of binding energy is as follows: Monolaurin < Plaunotol < Caryophyllene < Penconazole < Flusilazole < Ipconazole < Phenamacril < Carbendazim. Similarly, in the case of  $\beta$ -tubulin, the molecule follows the order as follows: Bisabolene <

Crassinervic acid < Ametocradin < Plaunotol < Dodine < Iaconazole < Carbendazim < Phenamacril. When screened against  $\gamma$ -tubulin, the binding energy data showed the order of Flusilazole < Metalaxyl < Monolaurin < Citronellol < Gramine < Phenamacril < Iaconazole < Carbendazim (Table 2).

When screened against the first gene of the NRPS31 gene cluster that is FFUJ\_00005, the binding energy follows the order Linolenic acid < Monocaprin < Monolaurin < Thymol < p-cymene < Phenamacril < Carbendazim < Iaconazole. Similar case is with the second gene that is FFUJ\_00006 the binding energy is in the order Phytol < Plaunotol < Oleic acid < Linolenic acid < Nerolidol < Phenamacril < Iaconazole < Carbendazim. Also when screened against FFUJ\_00007 the molecular binding energy follows the order Folicanthine < 10-Hydroxy-*cis*-12-octadecenoic acid < Phytol < Plaunotol < Oleic acid < Phenamacril < Iaconazole < Carbendazim. Similarly, preferable binding energy for FFUJ\_00008 was also estimated which follows the order Plaunotol < Phytol < Undecylenic acid < Kitazin < Iaconazole < Propineb < Carbendazim < Phenamacril. Similarly, for FFUJ\_00010, the preferable binding energy follows the order of 10-Hydroxy-*cis*-12-octadecenoic acid < Aduncumene < Terpinene < Plaunotol < Citronellol < Iaconazole < Phenamacril < Carbendazim. There is no difference for FFUJ\_00011 where binding energy follows the order of Nerolidol < Monolaurin < Gramine < Thiram < Calycanthine < Phenamacril < Carbendazim < Iaconazole while, for FFUJ\_00013, the order displays Monocaprin < Geraniol < Thujone < Bisabolene < Citronellol < Iaconazole < Carbendazim < Phenamacril (Table 2).

#### Ligand Efficiency (LE) and Lipophilic Ligand Efficiency (LLE)

Ligand efficiency and lipophilic ligand efficiency have been considered important factors to assess the drug likeness characteristics of a molecule. The concept of LE and LLE is a useful metric in the area of discovery of lead molecule and its optimizations. LE gives an estimate of the free binding energy per unit heavy atoms present in the molecule while LLE combines the potency and lipophilicity as the estimate to measure the efficiency of a lead molecule binding to a given target utilizing its lipophilicity.<sup>20,21</sup> Considering ‘++’ to be highly effective and ‘-’ to be least effective (Table 2), the order of ligand efficiency and lipophilic ligand efficiency determined as monolaurin > plaunotol > caryophyllene > flusilazole

> penconazole > ipconazole > penamacril > carbendazim for  $\alpha$ -tubulin; while bisabolene > crassinervic acid > ametocradin > plaunotol > dodine > ipconazole > penamacril > carbendazim for  $\beta$ -tubulin and citronellol > gramine > monolaurin > metalaxyl > flusilazole > ipconazole > penamacril > carbendazim for  $\gamma$ -tubulin.

Whereas, in NRPS31 gene cluster the order is, linolenic acid > thymol > p-cymene > monocaprin > monolaurin > ipconazole > penamacril > carbendazim for FFUJ\_00005, plaunotol > nerolidol > oleic acid > phytol > linolenic acid > ipconazole > penamacril > carbendazim for FFUJ\_00006, folicanthine > 10-hydroxy-*cis*-12-octadecenoic acid > plaunotol > phytol > oleic acid > ipconazole > penamacril > carbendazim for FFUJ\_00007, propineb > undecylenic acid > plaunotol > kitazin > phytol > ipconazole > carbendazim > penamacril for FFUJ\_00008, aduncumene > 10-Hydroxy-*cis*-12-octadecenoic acid > terpinene > citronellol > plaunotol > phenamacril > ipconazole > carbendazim for FFUJ\_00010, thiram > gramine > nerolidol > monolaurin > calycanthine > phenamacril > ipconazole > carbendazim for FFUJ\_00011 and geraniol > thujone > citronellol > bisabolene > monocaprin > phenamacril > ipconazole > carbendazim for FFUJ\_00013.

#### Interactions with Protein Complexes

Upon evaluation of the molecular interactions among the ligand-protein complexes, many different types of bonds were identified that are responsible for the effective binding affinity of the ligand toward the target proteins (Table 3).

#### Tubulin Protein Complex

$\beta$ -Caryophyllene@ $\alpha$ -tubulin interaction [eighteen non-bonding interactions comprising of all hydrophobic bonds (one  $\pi$ -sigma, nine alkyl, and eight  $\pi$ -alkyl bonds)] > ametocradin@ $\beta$ -tubulin interaction [sixteen non-bonding interactions including eight H-bonding (all conventional H-bonds) and eight hydrophobic bonding (one alkyl and seven  $\pi$ -alkyl bonds)] > flusilazole@ $\alpha$ -tubulin [eleven non-bonding interactions comprising of one H-bonding (conventional H-bonds), one electrostatic bond ( $\pi$ -cation) and nine hydrophobic interactions (two  $\pi$ - $\pi$  stacked, three  $\pi$ - $\pi$  T shaped and four  $\pi$ -alkyl bonds)] > monolaurin@ $\gamma$ -tubulin interaction [six non-bonding interactions out of which five are H-bonding (four conventional H-bonds and one C-H bond) and one hydrophobic bond (alkyl bond)].

Table 3 — Molecular interactions of flexible ligand docking with the most effective moieties against the  $\alpha$ -tubulin protein

Target-ligand interaction	Interaction Between	Distance	Category	Type
$\alpha$ -tubulin@ $\beta$ -caryophyllene	:CARY:C13 - :TYR24	3.59037	Hydrophobic	$\pi$ -Sigma
	:CYS25 - : CARY	4.29635	Hydrophobic	Alkyl
	: CARY:C4 - :ILE30	4.26516	Hydrophobic	Alkyl
	: CARY - :ILE30	4.44728	Hydrophobic	Alkyl
	: CARY - :PRO63	5.35234	Hydrophobic	Alkyl
	: CARY:C14 - :ILE30	4.45883	Hydrophobic	Alkyl
	: CARY:C14 - :PRO63	4.15906	Hydrophobic	Alkyl
	: CARY:C15 - :CYS25	4.47692	Hydrophobic	Alkyl
	: CARY:C15 - :PRO63	4.43327	Hydrophobic	Alkyl
	: CARY:C15 - :LEU86	4.62828	Hydrophobic	Alkyl
	:TRP21 - : CARY:C13	4.27872	Hydrophobic	$\pi$ -Alkyl
	:TRP21 - : CARY:C15	4.67221	Hydrophobic	$\pi$ -Alkyl
	:TRP21 - : CARY:C13	4.48641	Hydrophobic	$\pi$ -Alkyl
	:TYR24 - : CARY	5.09918	Hydrophobic	$\pi$ -Alkyl
	:HIS28 - : CARY:C4	5.09797	Hydrophobic	$\pi$ -Alkyl
	:TYR61 - : CARY:C4	4.03231	Hydrophobic	$\pi$ -Alkyl
	:TYR61 - : CARY	5.19005	Hydrophobic	$\pi$ -Alkyl
	:TYR61 - : CARY:C14	4.72199	Hydrophobic	$\pi$ -Alkyl
$\alpha$ -tubulin@flusilazole	:TYR61:OH - :FLUS:N4	2.89926	Hydrogen Bond	Conventional Hydrogen Bond
	:ARG64:NH1 - : FLUS	3.68388	Electrostatic	$\pi$ -Cation
	:TYR24 - : FLUS	3.70126	Hydrophobic	$\pi$ - $\pi$ -Stacked
	:HIS28 - : FLUS	3.9767	Hydrophobic	$\pi$ - $\pi$ -Stacked
	:TRP21 - : FLUS	5.50573	Hydrophobic	$\pi$ - $\pi$ -T-shaped
	:TRP21 - : FLUS	5.5467	Hydrophobic	$\pi$ - $\pi$ -T-shaped
	:TYR61 - : FLUS	4.78639	Hydrophobic	$\pi$ - $\pi$ -T-shaped
	:TYR24 - : FLUS:C22	5.02739	Hydrophobic	$\pi$ -Alkyl
	:HIS28 - : FLUS:C22	4.41467	Hydrophobic	$\pi$ -Alkyl
	: FLUS - :ILE30	5.14184	Hydrophobic	$\pi$ -Alkyl
$\alpha$ -tubulin@carbendazim	:FLUS - :PRO63		Hydrophobic	$\pi$ -Alkyl
	:TRP21:NE1 - :CARB:N3	3.2728	Hydrogen Bond	Conventional Hydrogen Bond
	:ARG64:N - : CARB:O2	2.81432	Hydrogen Bond	Conventional Hydrogen Bond
	:ARG64:CD - : CARB:O2	3.02876	Hydrogen Bond	Carbon Hydrogen Bond
	: CARB:C14 - :VAL4:O	3.33689	Hydrogen Bond	Carbon Hydrogen Bond
	: CARB:C14 - :SER6:OG	3.20775	Hydrogen Bond	Carbon Hydrogen Bond
	: CARB:C14 - :ARG64:O	3.29288	Hydrogen Bond	Carbon Hydrogen Bond
	: CARB - :TYR24	4.77412	Hydrophobic	$\pi$ - $\pi$ -Stacked
	:ALA65 - : CARB:C14	4.19031	Hydrophobic	Alkyl
	: CARB:C14 - :ARG64	4.63053	Hydrophobic	Alkyl
	:TRP21 - : CARB:C14	4.65655	Hydrophobic	$\pi$ -Alkyl
	: CARB - :PRO63	5.14935	Hydrophobic	$\pi$ -Alkyl
	: CARB - :CYS25	5.27259	Hydrophobic	$\pi$ -Alkyl
: CARB - :ILE30	5.199	Hydrophobic	$\pi$ -Alkyl	
: CARB - :PRO63	4.98196	Hydrophobic	$\pi$ -Alkyl	

Note: CARY-  $\beta$ -caryophyllene, FLUS- Flusilazole, CARB- Carbendazim

#### NRPS31 Gene Cluster Complex

Kitazin@FFUJ\_00008 interaction [twelve non-bonding interactions comprising of two H-bonding (both conventional H-bonds), nine hydrophobic bonding (four  $\pi$ -alkyl, three alkyl, one  $\pi$ -sigma and one amide- $\pi$  stacked) and one other ( $\pi$ -sulphur bond)] >

nerolidol@FFUJ\_00011 interaction [nine non-bonding interactions comprising of two H-bonding (one conventional H-bond and one C-H bond) and seven hydrophobic interactions (one  $\pi$ -sigma, two alkyl and four  $\pi$ -alkyl)] > 10-Hydroxy-*cis*-12-octadecenoic aci@FFUJ\_00007 interaction [eight non-bonding

interactions including three H-bonding (all conventional H-bond) and five hydrophobic bonding (three alkyl and two  $\pi$ -alkyl bonds)] > linolenic acid@FFUJ\_00005 [seven non-bonding interactions including three H-bonding (all conventional H-bonds) and four hydrophobic bonding (one alkyl and three  $\pi$ -alkyl bonds)]-geraniol@FFUJ\_00013 [seven non-bonding interaction comprising of two H-bonding (both conventional H-bonds) and five hydrophobic bonding (two alkyl and three  $\pi$ -alkyl)] > oleic acid@FFUJ\_00006 interaction [six non-bonding interactions consisting of two H-bonding (both conventional H-bonds) and four hydrophobic bonding (all alkyl bonds)] > 10-hydroxy-*cis*-12-octadecenoic acid@FFUJ\_00010 interaction [five non-bonding interactions including four H-bonding (all conventional H-bond) and one hydrophobic bonding ( $\pi$ -alkyl bond)].

#### Target-Ligand Interactions

***$\beta$ -Caryophyllene@ $\alpha$ -tubulin:*** All hydrophobic bonds are equally distributed of allyl hydrophobic bonds and  $\pi$ -allyl hydrophobic bonds. Residue TYR 24 plays a major role in the stabilization of the complex by forming a  $\pi$ -sigma bond and a  $\pi$ -alkyl bond with the caryophyllene scaffold conferring stability to the target ligand complex. All the residues (TYR24, CYS25, ILE30, PRO63, LEU86, TRP21, HIS28, TYR61) were found to lie within the first motif (Tubulin) of  $\alpha$ -tubulin but no any residue was found to occur in the other two motifs (Tubulin\_C, Tubulin\_3).

***Ametoctradin@ $\beta$ -tubulin:*** Two crucial conventional H-bonding interactions of the ametoctradin molecule with the amino acid residue TYR 227 and PRO 272 give a bridge-like stability to the overall basis of the selection of compounds across the molecular targets. All the residues (TYR227, PRO272, PRO358, LEU361) were found to lie within the second motif (Tubulin\_C) of  $\beta$ -tubulin but no residue was found to occur in other motifs (Tubulin, Misat\_Tub\_Seg II, Tubulin\_2, Tubulin\_3).

***Monolaurin@ $\gamma$ -tubulin:*** The four O-atoms of the monolaurin compound form four conventional H-bonds forming a very stable on-site confirmation during the complex formation. Three residues (CYS13, ASN207, VAL181) were found to lie within the first motif (Tubulin) of  $\gamma$ -tubulin while one residue (ASN229) was not found to occur in any motifs. Also, no residue was found to occur in other motifs (Misat\_Tub\_Seg II, Tubulin\_C, Tubulin\_3).

***Linolenic acid@FFUJ00005:*** Four terminal H-bonds at the active terminal and four terminal hydrophobic

bonds at the alkyl terminal end gives the much needed stability to the molecular conformation in the protein target site and thus the good predicted activity. Only two residues that are HIS232 and TYR527 were found in FAD\_Binding\_4 and BBE motifs respectively while other residues (VAL469, LYS470, LEU487, TRP481,) were not found to occur in any motifs. Also, no residue was found to occur in another motif (Cytokine-bind).

***Oleic acid@FFUJ00006:*** One terminal H-bond at the hydroxyl O-atom of the acidic terminal and two hydrophobic bonds at the alkyl terminal and spells the reason for the activity profile prediction for the oleic acid@FFUJ00006 complex. Furthermore, the structural comparison between the linolenic acid@FFUJ00005 and oleic acid@FFUJ00006 complexes gives a clear understanding about how the presence of more number of bonds on the terminal ends of the molecule induces stability while its binding to the sites will have a greater impact on the stability of the complex. All the residues (GLY27, CYS15, LEU18, GLY27) were found to lie within the first motif (p450) of FFUJ\_00006.

***10-Hydroxy-*cis*-12-octadecenoic acid@FFUJ\_00007:*** The reason behind the excellent predicted activity of the molecule against the target site seems to be the ample number of hydrophobic interactions with the interacting amino acid residues and the H-bonded terminal acid moiety of the molecule. All the residues (ARG228, MET226, LEU312, ALA513, LYS503, PHE504, PHE514) were found to lie within the first motif (p450) of FFUJ\_00007.

***Kitazin@FFUJ00008:*** Kitazin shows a variety of hydrophobic interactions ranging from  $\pi$ -sigma,  $\pi$ -sulfur,  $\pi$ -amide and  $\pi$ -alkyl interactions wherein  $\pi$ -alkyl played the dominant role in terms of overall presence. The amino acid residue CYS 138 played a major role in determination of the lowered energy conformation of the kitazin molecule on the target site by getting involved in the hydrophobic interaction present at both the terminals of the molecule. Only two residues that is ILE60 and ARG61 were found in Dimerization motif while other residues (ARG110, HIS57, CYS138, SER139, PHE129, TYR141, CYS138) was not found to occur in any motifs. Also, no residue was found to occur in other motifs (Methyltransf\_2, Methyltransf\_31).

***10-Hydroxy-*cis*-12-octadecenoic acid@FFUJ\_00010:*** The good predicted activity of the long chain compound seems to be the presence of very strong H-bonds at the carbonyl terminal end and the hydroxyl moiety at the central part of the molecule, which in turn was

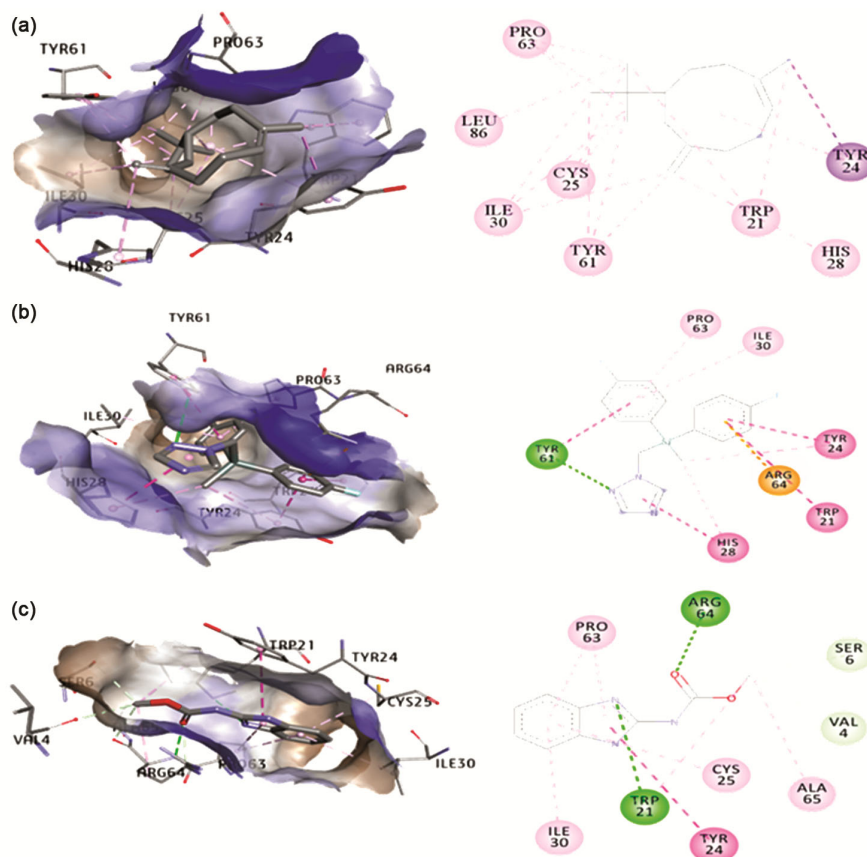


Fig. 1 — 3D and 2D representations of the best effective molecule: (a)  $\beta$ -caryophyllene, (b) flusilazole with respect to control, (c) carbendazim

complemented by the presence of a sole hydrophobic bond at the alkyl terminal end of the molecule. Only two residues that is ASN479 and ARG503 were found in FAS\_I\_H motif while other residues (ARG549, PHE553) was not found to occur in any other motifs (Fas\_Alpha\_ACP, ketoacyl-synt, ketoacyl-synt\_C, GDP\_Man\_Dehyd, Thiolase\_N).

**Nerolidol@FFUJ\_00011:** The potential activity of the alcohol seems to be significant due to the presence of very strong conventional H-bonds and C-H bond with ASN 129 and HIS70 respectively while other interactions also adds to its stability such as  $\pi$ -sigma, alkyl and  $\pi$ -alkyl with HIS164 and ALA127. All the residues (ASN129, HIS70, HIS164, ALA127) except one (TRP331) were found to lie within the first motif (Aminotran\_4) of FFUJ\_00011.

**Geraniol@FFUJ\_00013:** The activity is attributed to the presence of bonds such as conventional H-bond,  $\pi$ -alkyl, alkyl. None of any residue (SER138, PRO115, ALA137, PRO134, PHE111, PHE117) were found in any motifs (P5CR\_Dimer, F420\_oxidored) of FFUJ\_00013.

#### Selective Binding Affinity of $\alpha$ -tubulin

$\alpha$ -Tubulin binding activity was shown to be higher by the studied compounds, which led us to choose the best  $\alpha$ -tubulin-compound complexes for further detailed interaction analysis and compare the same to  $\alpha$ -tubulin@carbendazim complex in order to unearth the reason for better activity of these cherry-picked compounds.

The molecule when binds to the  $\alpha$ -tubulin protein structure it formed a very stable complex comprising of eighteen favourable non-bonding interactions. Among the eighteen non-bonding interactions present, all the bonds were reported to be hydrophobic interactions comprising various other different kinds of bonds such as one  $\pi$ -sigma, nine alkyl and eight  $\pi$ -alkyl bonds interaction. The residue TYR-61, TYR-24, CYS-25, LEU-86, HIS-28, TRP-21, PRO-63 and ILE-30 played a vital role in the interaction with the incoming ligands (Fig. 1a). The  $\beta$ -caryophyllene@ $\alpha$ -tubulin complex exhibited a binding energy of  $-40.5 \text{ kcal mol}^{-1}$  with good positive ligand efficiency

and a remarkable binding affinity in the range of 16.05–1595.40 nM periods.

The molecule when binds to the  $\alpha$ -tubulin protein structure it formed a very stable complex comprising of eleven favourable non-bonding interactions. Among the eleven non-bonding interactions present, one was found to be conventional H-bond, other one was electrostatic  $\pi$ -cation interaction and rest others were nine hydrophobic interactions comprising various other different kinds of bonds such as two  $\pi$ - $\pi$  stacked interactions, three  $\pi$ - $\pi$  T-shaped interactions and four were found to be  $\pi$ -alkyl interaction. The residue PRO-63, ILE-30, TRP-21, TYR-61, ARG-64, TYR-24, HIS-28 played a vital role in the interaction with the incoming ligands which was bound to the GTPase domain motive of the  $\alpha$ -tubulin protein (Fig. 1b). All the residues were found to lie within the first motif (Tubulin) of  $\alpha$ -tubulin but no any residue was found to occur in other two motifs (Tubulin\_C, Tubulin\_3). The flusilazole@ $\alpha$ -tubulin complex exhibited a binding energy of  $-35.5 \text{ kcal mol}^{-1}$  with good positive ligand efficiency and a remarkable binding affinity in the range of 69.4–6896.25 nM period.

### Molecular Dynamics

This report presents the findings of a study on the  $\alpha$ -tubulin protein in the *F. fujikuroi* fungus. The protein's structure was determined using homology modeling, and mutational analysis indicated that point mutations could have an impact on the protein's stability and its relationship with its function. The study also investigated the dynamics of the interaction between the  $\alpha$ -tubulin protein and three fusion entry inhibitors: carbendazim (a commonly used fungicide), flusilazole (a synthetic lead predicted through virtual screening), and  $\beta$ -caryophyllene (a natural lead predicted through virtual screening). Molecular dynamics (MD) simulations were performed to analyze the behavior of the protein and protein-ligand complexes. The MD simulations showed that all three inhibitors stabilized the  $\alpha$ -tubulin protein, with carbendazim exhibiting weaker stabilization compared to the other two compounds. The dynamics of the  $\alpha$ -tubulin@carbendazim,  $\alpha$ -tubulin@ $\beta$ -caryophyllene, and  $\alpha$ -tubulin@flusilazole complexes were further examined using GROMACS software. Various parameters such as energy values, RMSD values, and radius of gyration were calculated during the MD simulations to assess the stability and convergence of the native  $\alpha$ -tubulin protein and the protein-ligand

complexes. The analysis of the RMSD values, which measure the deviation of the protein's structure over time, demonstrated a consistent and steady trajectory, indicating stabilization and convergence. The RMSD values were calculated using an equation.<sup>22</sup>

$$RMSD(t_1, t_2) = \left[ \frac{1}{N} \sum_{i=0}^n (r_i(t_1) - r_i(t_2))^2 \right]^{\frac{1}{2}}$$

where,  $t_2$  = time of the reference structure,  $t_1$  = time point in the simulation,  $r_i$  = atom position  $i$  at a particular time and  $N$  = number of atoms.

The RMSD plot (Fig. 2) demonstrates that the MD simulation of the native  $\alpha$ -tubulin protein was conducted for a duration of 30 ns. It is observed that the predicted protein structure is less stable than the complex structures during the simulation. Without the presence of a lead molecule, the apo-protein exhibits clear instability. The maximum RMSD value for the native  $\alpha$ -tubulin protein occurs at 23 ns, reaching 1.01872 Å. However, the RMSD plot stabilizes at 30 ns. Similarly, MD simulations were performed for the  $\alpha$ -tubulin protein-ligand complexes, which also demonstrated stability around 28 ns. Comparing the RMSD values, it is evident that the complexes are more stable than the native  $\alpha$ -tubulin protein. The  $\alpha$ -tubulin@ $\beta$ -caryophyllene complex exhibits a maximum RMSD value of 1.31494 Å at approximately 25 ns, while the  $\alpha$ -tubulin@flusilazole complex reaches a maximum RMSD value of 1.22257 Å around 27 ns. For the  $\alpha$ -tubulin@carbendazim complex, the maximum RMSD value is 1.41312 Å at 32.4 ns. Notably, the  $\alpha$ -tubulin@flusilazole complex reaches stability earliest, at around 17 ns. The RMSD trajectories of the

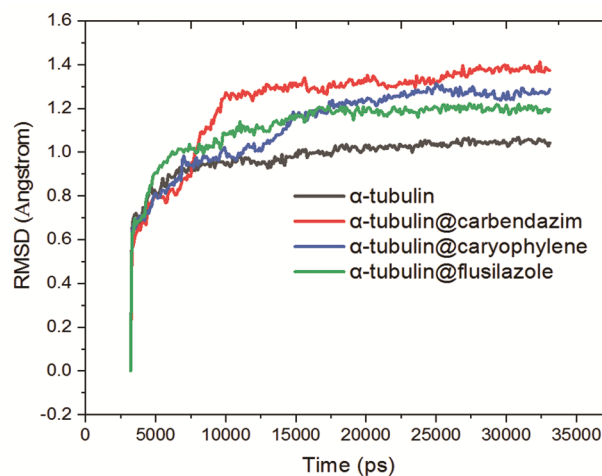


Fig. 2 — RMSD graph of the apoprotein with the three ligand molecules resulting from the MD simulation of the apo-protein and the three ligands

$\alpha$ -tubulin@ $\beta$ -caryophyllene complex stabilize at 24 ns, while the  $\alpha$ -tubulin@carbendazim complex stabilizes at approximately 25 ns. The RMSD fluctuations of the apo-protein and complexes are observed initially but eventually stabilize after 40 ns, except for the mentioned complexes.

The order of stabilization for the  $\alpha$ -tubulin protein follows the trend:  $\alpha$ -tubulin@flusilazole >  $\alpha$ -tubulin@ $\beta$ -caryophyllene >  $\alpha$ -tubulin@carbendazim, as indicated by the RMSD values. The energy plot (Fig. 3) further supports these findings. The total energy of the protein and complexes throughout the MD simulations is analyzed. It is evident that the binding of inhibitor molecules, such as  $\alpha$ -tubulin@carbendazim (-22,986.30 kcal/mol),  $\alpha$ -tubulin@flusilazole (-22,890.20 kcal/mol), and  $\alpha$ -tubulin@ $\beta$ -caryophyllene (-22,986.30 kcal/mol), enhances the overall thermodynamic stability of the complexes compared to the apo-protein (-22,716.20 kcal/mol).

To assess the compactness of a protein, the radius of gyration (Rg) was determined. Rg is a measure of the root mean square distance between a specific atom or group of atoms and the protein's center of mass. The calculation of Rg involves applying an equation:<sup>23</sup>

$$R_g = \left( \frac{\sum_i r_i^2 m_i}{\sum_i m_i r_i} \right)$$

where,  $r_i$  = perpendicular distance from the axis of rotation and  $m_i$  is the molecular mass.

According to Kumar *et al.* (2014)<sup>24</sup>, a protein that is stably folded exhibits a consistent and unchanging radius of gyration (Rg) throughout the simulation.

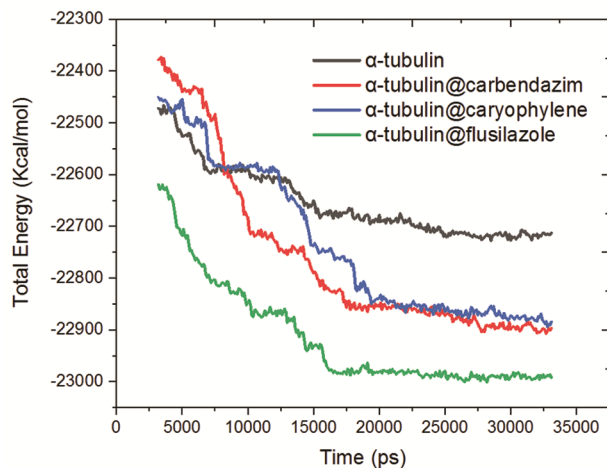


Fig. 3 — Energy plot of the apo-protein with the three ligand molecules derived from the MD simulation of the apo-protein and the three ligands

Conversely, variations in Rg indicate the onset of protein unfolding. In this study, the Rg values were plotted against time for  $\alpha$ -tubulin,  $\alpha$ -tubulin@ $\beta$ -caryophyllene,  $\alpha$ -tubulin@flusilazole, and  $\alpha$ -tubulin@carbendazim (Fig. 4). The Rg values obtained for these states were 21.24, 21.21, 21.09, and 21.14 Å, respectively.

The Rg value for the apo-protein was higher compared to the complexes formed with  $\beta$ -caryophyllene, flusilazole, and carbendazim. This suggests that the  $\alpha$ -tubulin@ $\beta$ -caryophyllene,  $\alpha$ -tubulin@flusilazole, and  $\alpha$ -tubulin@carbendazim complexes were stabilized, as these compounds are known to serve as positive controls for evaluating drug-like properties.<sup>25</sup> The plot in Fig. 4 demonstrates that the protein maintained stable folding states in all three scenarios:  $\alpha$ -tubulin alone and when complexed with carbendazim, flusilazole, and  $\beta$ -caryophyllene. The radius of gyration results, as depicted in Fig. 4, support the findings from the RMSD graph, indicating that, except for the  $\alpha$ -tubulin@carbendazim complex, all the complexes exhibited increased stability compared to the apo-protein, with minimal fluctuations observed.

The RMSF (Root Mean Square Fluctuation) graph of the apo- and complex proteins, as shown in Fig. 5, assisted in keeping track of each protein residue and the complex to examine its dynamic behaviour. The RMSF values were used to analyse and evaluate the variations in structural behaviour and flexibility between apo and complex proteins. From Fig. 5, it is clear that the apo-protein and stable  $\alpha$ -tubulin@ $\beta$ -caryophyllene and  $\alpha$ -tubulin@flusilazole complexes exhibit greater fluctuations of 0.7 to 0.8 in the areas about 25–50, 175–275, and 375–430. Greater variation of the  $\alpha$ -tubulin@carbendazim complex, ranging from 1.12 to 1.4, was seen in the areas 25–75, 125–137, 211–224, 273–294, 322–326 and 361–369. Additionally, it was found that the stable  $\alpha$ -tubulin@ $\beta$ -caryophyllene and  $\alpha$ -tubulin@flusilazole complexes as well as the native  $\alpha$ -tubulin protein exhibit minor changes for all other residues.

When comparing how well a solute dissolves in various solvents, one method is to take the free energy of transfer into account. This number effectively enables comparison of solvation energies without taking into account interactions between solutes and solvents. Consequently, the free energy of solvation for the apo-protein and the three complexes was calculated using MD simulation, and it was found that the solvation energy (polar contribution) for the apo-protein and the stable  $\alpha$ -tubulin@ $\beta$ -caryophyllene

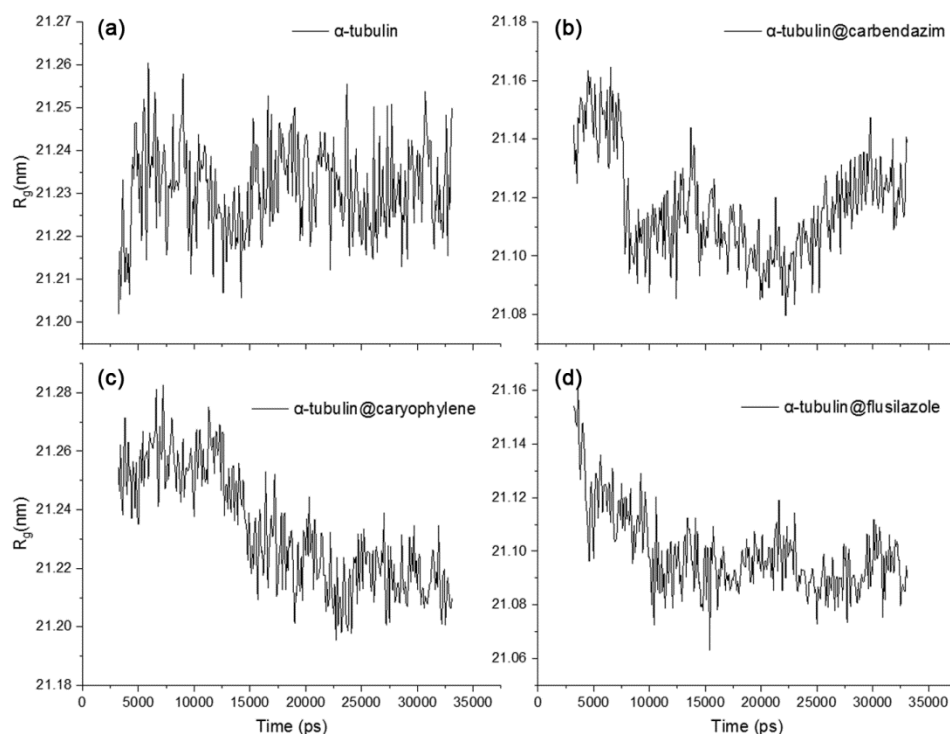


Fig. 4 — Graph depicting the  $R_g$  values for the native: (a)  $\alpha$ -tubulin, (b)  $\alpha$ -tubulin@carbendazim, (c)  $\alpha$ -tubulin@ $\beta$ -caryophyllene, and (d)  $\alpha$ -tubulin@flusilazole complexes throughout the MD simulation protocol

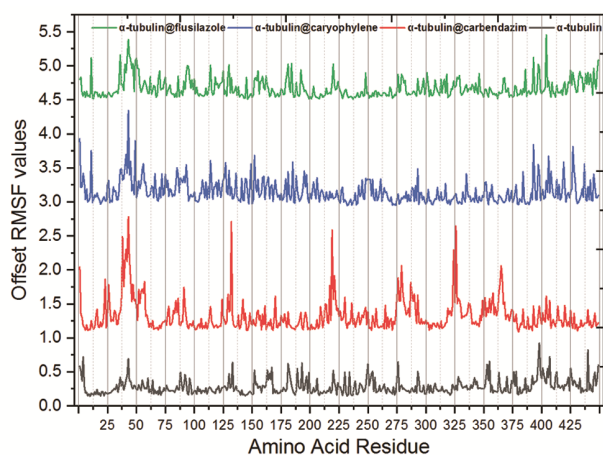


Fig. 5 — RMSF graph resulting from the trajectory analysis of MD simulation of the apo-protein with the three ligand molecules

and  $\alpha$ -tubulin@flusilazole complexes were, respectively,  $-7504.104\text{kT}$ ,  $-7603.213\text{kT}$ ,  $-7556.993\text{kT}$ , and  $-7722$ . Strong solvent-solute interactions improved the process of solvation, as is seen from the solvation energy calculation's outcome.

Based on the results of this study, it can be concluded that flusilazole and caryophyllene show promise as lead compounds for potential entry inhibitors against *F. fujikuroi* in the context of managing bakanae disease

in rice. Further comprehensive experimental investigations, such as 3-D QSAR (quantitative structure-activity relationship), gene expression analysis, and cytotoxicity studies, are warranted to gain a deeper understanding of the inhibitory mechanism of flusilazole and caryophyllene, as well as their derivatives, in combating bakanae disease. These additional studies will provide valuable insights into the mode of action and potential development of these compounds as effective treatments for the disease.

The majority of the compounds formed a stable interaction complex between themselves, as indicated by the predicted activity of the compounds against the target proteins of *F. fujikuroi*, and this finding is again supported by the specifics of the non-bonding interaction-based chemistry, as shown in Table 3 and Fig. 1. The following is the pesticide-likeness rule of Hao *et al.*<sup>26</sup>: Out of the 170 compounds examined, the best compounds had  $\text{MW} \leq 435$  Da,  $\log$  of the predicted octanol-water partition coefficients ( $\text{CLogP}$ )  $\leq 6$ ,  $\text{HBA} \leq 6$ ,  $\text{HBD} \leq 2$ ,  $\text{ROB} \leq 9$ , and the number of aromatic bonds (ARB) 17.14.<sup>(27,28)</sup> The best compounds emerged out for each of the ten target sites were: Caryophyllene ( $\alpha$ -tubulin), ametoctradin ( $\beta$ -tubulin), monolaurin ( $\gamma$ -tubulin), linolenic acid (FFUJ\_00005), oleic acid (FFUJ\_00006), 10-Hydroxy-*cis*-12-octadecenoic acid

(FFUJ\_00007), kitazin (FFUJ\_00008), 10-Hydroxy-*cis*-12-octadecenoic acid (FFUJ\_00010), nerolidol (FFUJ\_00011), and geraniol (FFUJ\_00013). The most striking feature of the binding energy results of all the ten target sites was that plaunotol and monolaurin showed the most favourable binding towards FFUJ\_00008 and  $\alpha$ -tubulin target sites, respectively. The likelihood of discovering hits is really low given the vast chemical space of drug-like compounds. Thus, methods have been developed to reduce affinity-biased selection, and instead of optimisation that favours big ligands, the emphasis should be on choosing molecules that make the most use of their atoms.<sup>29-31</sup> Thus, came into existence the usage of LLE and LE, as guiding indices towards chemical discovery. Furthermore, lowest  $pK_i$  range (indicating highest potency of an inhibitor) were found for the  $\beta$ -caryophyllene@ $\alpha$ -tubulin complexes, which further establishes the fact that  $\beta$ -caryophyllene may easily be touted as the best putative inhibitor of the lot.<sup>32,33</sup>

#### Fungicidal Efficacy

Based on the screening results against ten vital target proteins of *F. fujikuroi*, two molecules,  $\beta$ -caryophyllene and flusilazole were selected and tested for their efficacy to control the pathogen. Both the molecules proved to be highly effective than that of the positive control, carbendazim. Wide range of inhibition (85.31–56.37%) was observed at the concentration gradient of 100–6.25

$\mu\text{g/mL}$  in case of  $\beta$ -caryophyllene while for flusilazole inhibited 83.08% to 40.12% at the concentration gradient of 500–31.25  $\mu\text{g/mL}$ . However, at the same concentrations carbendazim (positive control) inhibited 67.52–22.33% mycelial growth. In terms of effective concentration for 50% inhibition of mycelial growth ( $EC_{50}$ ),  $\beta$ -caryophyllene exhibited highest efficacy with only 3.29  $\mu\text{g/mL}$  concentration. While, flusilazole and carbendazim were moderately effective against *F. fujikuroi* with the  $EC_{50}$  64.12 and 178.77  $\mu\text{g/mL}$ , respectively (Table 4, Fig. 6 & 7).

The outcome of the detail molecular docking and dynamics studies was further validated through *in-vitro* antifungal assays. Surprisingly, the pathogen, *F. fujikuroi* was found highly sensitive to  $\beta$ -caryophyllene. Notwithstanding, the performance of  $\beta$ -caryophyllene was even better than both the synthetic compounds, flusilazole and carbendazim. Furthermore,  $\beta$ -caryophyllene and flusilazole showed higher binding energy while interacting with most of the selected major proteins of *Fusarium*. The correlation between *in-silico* and *in-vitro* efficacy of these selected molecules has been established in order to define inhibition of various major target proteins causing virulence.

*Bakanae* disease of rice caused by *F. fujikuroi* resulted havoc yield loss through its primary and secondary infections during vegetative stages by conidia.<sup>34</sup> Literature reports indicated major

Table 4 — Probit analysis of antifungal bioefficacy data of best selected molecule against *F. fujikuroi* at different concentration gradient

Samples	$LC_{50}$ ( $\mu\text{g/mL}$ )	95% Confidence limit ( $\mu\text{g/mL}$ )		Slope $\pm$ SE	Intercept $\pm$ SE	$(\chi^2)$
		Lower	Upper			
$\beta$ -Caryophyllene	3.29	1.18	5.70	$0.72 \pm 0.14$	$-0.37 \pm 0.20$	0.43
Flusilazole	64.12	32.53	97.28	$1.06 \pm 0.14$	$-1.93 \pm 0.30$	3.10
Carbendazim	178.77	138.45	242.07	$1.03 \pm 0.14$	$-2.32 \pm 0.30$	0.15

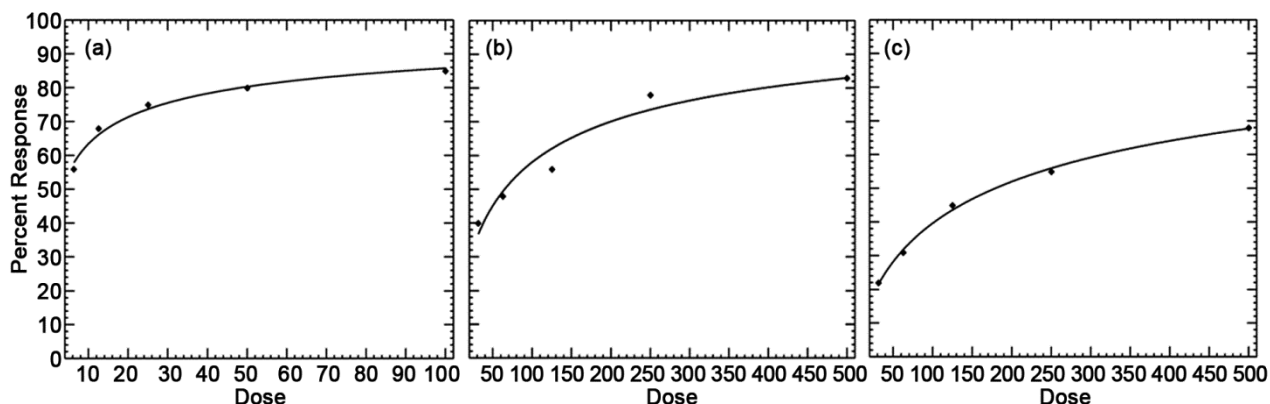


Fig. 6 — Dose response curve of  $\beta$ -caryophyllene (a), flusilazole (b) and carbendazim (c) against *F. fujikuroi* at different concentration gradient plotted as percent inhibition versus dose (ppm)

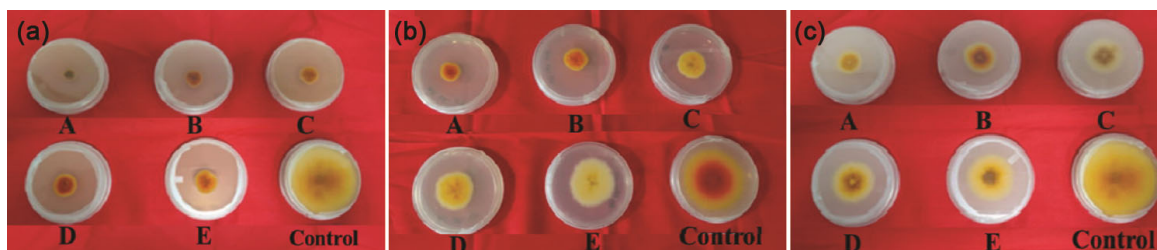


Fig. 7 — Effect of best effective fungicidal molecules,  $\beta$ -caryophyllene (a), flusilazole (b) and carbendazim (c) against *F. fujikuroi* by poisoned food assay technique at different concentration gradient of  $\beta$ -caryophyllene (A = 100 ppm, B = 50 ppm, C = 25 ppm, D = 12.5 ppm, E = 6.25 ppm), flusilazole and carbendazim (A = 500 ppm, B = 250 ppm, C = 125 ppm, D = 62.5 ppm, E = 31.25 ppm)

difficulties and challenges to control the pathogen completely.<sup>35</sup> Infected seeds are the primary source of the infection which disseminates both internally and externally, therefore, a holistic approach is required to control the pathogen.<sup>36</sup> Several literature suggests the effectiveness of carbendazim in the form of soil drenching and flusilazole in the form of seed soaking for 8 h to manage the pathogen effectively.<sup>37,38</sup> Although, bavistin (carbendazim 50% WP) is the most widely used fungicides in India<sup>33</sup> but there are several reports of developing resistance of *Fusarium* spp. against benzimidazole group of fungicides.<sup>5</sup> Additionally, several fungicides including carbendazim is on the verge of banning in India. Discrete reports are available about the effectiveness of plant derived essential oil components against the fungi.<sup>39</sup> Being an essential oil constituent,  $\beta$ -caryophyllene showed highest effectiveness to suppress the fungal growth and development in the present study which supports the findings of Wan *et al.*, 2020.<sup>(40)</sup> Fungicidal molecules with multidimensional functional properties inhibiting multiple target sites have been considered an option. In our study, a variety of compounds from natural and synthetic sources have been reported to possess substantial antifungal properties; however, mechanisms of their interaction with the target enzymes have not been explained clearly. The present study demonstrated screening and assessment of a wide library of natural and synthetic molecules using molecular docking and dynamics approach to discover the most potential compounds for the control of rice seed-borne pathogen, *F. fujikuroi*.

## Conclusions

In summary, two most potential fungicidal compounds namely,  $\beta$ -caryophyllene and flusilazole have been identified from comprehensive mining of 170 natural and synthetic molecules, respectively. Molecular modelling and dynamics approaches were used to demonstrate the detail mechanism of

interactions of the molecules with ten major target proteins of *F. fujikuroi* species complex, causal organism of bakanae disease of rice. Surprisingly, the best possible molecular interactions with maximum number of target proteins of the pathogen were observed with  $\beta$ -caryophyllene, which is far better than the recommended synthetic fungicide, carbendazim. Additionally, flusilazole was also found effective based on its molecular interactions with the target proteins. Further, experimental validations in order to prove fungicidal action of these molecules have also proved their effectiveness. However, further research is needed to develop suitable product(s) for further multi-locational field trials in the rice growing zones.

## Conflict of interests

The authors confirm no possible conflict of interest regarding the authorship, investigation, and publishing of the current article.

## Acknowledgement

The authors gratefully acknowledge, Indian Council of Agricultural Research-Indian Agricultural Research Institute (ICAR-IARI), New Delhi, India for providing research facilities and CII-SERB and UPL Ltd. for financial assistance.

## References

- Janevska S & Tudzynski B, Secondary metabolism in *Fusarium fujikuroi*: Strategies to unravel the function of biosynthetic pathways, *Appl Microbiol Biotechnol*, **102** (2018) 615–630.
- Bömke C & Tudzynski B, Diversity, regulation, and evolution of the gibberellin biosynthetic pathway in fungi compared to plants and bacteria, *Phytochemistry*, **70** (2009) 1876–1893.
- Bashyal B M, Aggarwal R, Sharma S, Gupta S & Singh U B, Single and combined effects of three *Fusarium* species associated with rice seeds on the severity of bakanae disease of rice, *J Plant Pathol*, **98** (2016) 405–412.
- Li M, Li T, Duan Y, Yang Y, Wu J, Zhao D, Xiao X, Pan X, Chen W, Wang J & Chen C, Evaluation of

- phenamacril and ipconazole for control of rice bakanae disease caused by *Fusarium fujikuroi*, *Plant Dis*, **102** (2018) 1234–1239.
- 5 Chen Y, Huang T T, Chen C J, Hou Y P, Zhang A F, Wang W X, Gao T C & Zhou M G, Sensitivity of *Fusarium verticillioides* isolates from rice to a novel cyanoacrylate fungicide, *Crop Prot*, **39** (2012) 106–109.
  - 6 Chen Z, Gao T, Liang S, Liu K, Zhou M & Chen C, Molecular mechanism of resistance of *Fusarium fujikuroi* to benzimidazole fungicides, *FEMS Microbiol Lett*, **357** (2014) 77–84.
  - 7 Wilson L & Jordan M A, Microtubule dynamics: taking aim at a moving target, *Chem Biol*, **2** (1995) 569–573.
  - 8 Erickson H P,  $\gamma$ -tubulin nucleation: template or protofilament?, *Nat Cell Biol*, **2** (2000) 93–95.
  - 9 Hansen F T, Gardiner D M, Lysøe E, Fuertes P R, Tudzynski B, Wiemann P, Sondergaard T E, Giese H, Brodersen D E & Sørensen J L, An update to polyketide synthase and non-ribosomal synthetase genes and nomenclature in *Fusarium*, *Fungal Genet Biol*, **75** (2015) 20–29.
  - 10 Niehaus E M, Münsterkötter M, Proctor R H, Brown D W, Sharon A, Idan Y, Oren-Young L, Sieber C M, Novák O, Pěňčík A & Tarkowská D, Comparative “omics” of the *Fusarium fujikuroi* species complex highlights differences in genetic potential and metabolite synthesis, *Genome Biol Evol*, **8** (2016) 3574–3599.
  - 11 Wiemann P, Sieber C M, Von Bargen K W, Studt L, Niehaus E M, Espino J J, Huss K, Michielse C B, Albermann S, Wagner D & Bergner S V, Deciphering the cryptic genome: Genome-wide analyses of the rice pathogen *Fusarium fujikuroi* reveal complex regulation of secondary metabolism and novel metabolites, *PLoS Pathog*, **9** (2013) 1–36.
  - 12 Zhang S Y, Dai D J, Wang H D & Zhang C Q, One-step loop-mediated isothermal amplification (LAMP) for the rapid and sensitive detection of *Fusarium fujikuroi* in bakanae disease through NRPS31, an important gene in the gibberellic acid bio-synthesis, *Sci Rep*, **9** (2019) 1–9.
  - 13 Jin J M, Lee S, Lee J, Baek S R, Kim J C, Yun S H, Park S Y, Kang S & Lee Y W, Functional characterization and manipulation of the apicidin biosynthetic pathway in *Fusarium semitectum*, *Mol Microbiol*, **76** (2010) 456–466.
  - 14 Kundu A, Dutta A, Mandal A, Negi L, Malik M, Puramchatwad R, Antil J, Singh A, Rao U, Saha S & Kumar R, A comprehensive *in vitro* and *in silico* analysis of nematocidal action of essential oils, *Front Plant Sci*, **11** (2021) 1995–2008.
  - 15 Dutta A, Mandal A, Kundu A, Malik M, Chaudhary A, Khan M R, Shanmugam V, Rao U, Saha S, Patanjali N & Kumar R, Deciphering the behavioral response of *Meloidogyne incognita* and *Fusarium oxysporum* toward mustard essential oil, *Front Plant Sci*, (2021) **12** 1791–1806.
  - 16 Laskowski R A, MacArthur M W, Moss D S & Thornton J M, PROCHECK: A program to check the stereochemical quality of protein structures, *J Appl Crystallogr*, **26** (1993) 283–291.
  - 17 Patil V S, Deshpande S H, Harish D R, Patil A S, Virge R, Nandy S & Roy S, Gene set enrichment analysis, network pharmacology and *in silico* docking approach to understand the molecular mechanism of traditional medicines for the treatment of diabetes mellitus, *J Protein Proteomics*, **11** (2020) 297–310.
  - 18 Singh R, Bhardwaj V & Purohit R, Identification of a novel binding mechanism of Quinoline based molecules with lactate dehydrogenase of *Plasmodium falciparum*, *J Biomol Struct Dyn*, **39** (2021) 348–356.
  - 19 Kamigauchi M, Kawanishi K, Sugiura M, Ohishi H & Ishida T,  $\gamma$ -Cyclodextrin as Inhibitor of the precipitation Reaction between Berberine and Glycyrrhizin in Decoctions of Natural Medicines: Interaction studies of Cyclodextrins with Glycyrrhizin and Glycyrrhetic Acid by 1H-NMR Spectroscopy and molecular-Dynamics Calculation, *Helvetica Chimica Acta*, **91** (2008) 1614–1624.
  - 20 Chen H, Zhou X, Gao Y & Zhou J, Fragment-based drug design: Strategic advances and lessons learned, in *Drug Discovery Technologies* (Elsevier Inc.) **2–8** (2017) 212–232.
  - 21 Scott J S & Waring M J, Practical application of ligand efficiency metrics in lead optimization, *Bioorg Med Chem*, **26** (2018) 3006–3015.
  - 22 Schreiner W, Karch R, Knapp B & Ilieva N, Relaxation estimation of RMSD in molecular dynamics immunosimulations, *Comput Math Methods Med*, **2012** (2012) 173521.
  - 23 Liu P, Lu J, Yu H, Ren N, Lockwood F E & Wang Q J, Lubricant shear thinning behavior correlated with variation of radius of gyration via molecular dynamics simulations, *J Chem Phys*, **147(8)** (2017) 084904.
  - 24 Kumar C V, Swetha R G, Anbarasu A & Ramaiah S, Computational analysis reveals the association of threonine 118 methionine mutation in PMP22 resulting in CMT-1A, *Adv bioinformatics*, **2014** (2014) 1–10.
  - 25 Madrid P B, Panchal R G, Warren T K, Shurtleff A C, Endsley A N, Green C E, Kolokoltsov A, Davey R, Manger I D, Gilfillan L & Bavari S, Evaluation of Ebola virus inhibitors for drug repurposing, *ACS Infect Dis*, **1(7)** (2015) 317–326.
  - 26 Hao G, Dong Q & Yang G, A comparative study on the constitutive properties of marketed pesticides, *Mol Inform*, **30** (2011) 614–622.
  - 27 Wang M Y, Wang F, Hao G F & Yang G F, FungiPAD: A free web tool for compound property evaluation and fungicide-likeness analysis, *J Agric Food Chem*, **67** (2019) 1823–1830.
  - 28 Cheng T, Zhao Y, Li X, Lin F, Xu Y, Zhang X, Li Y, Wang R & Lai L, Computation of octanol– water partition coefficients by guiding an additive model with knowledge, *J Chem Inf Model*, **47** (2007) 2140–2148.
  - 29 Raymond J L & Awale M, Exploring chemical space for drug discovery using the chemical universe database, *ACS Chem Neurosci*, **3** (2012) 649–657.
  - 30 Leach A R, Hann M M, Burrows J N & Griffen E J, Fragment screening: an introduction, *Mol Biosyst*, **2** (2006) 429–446.
  - 31 Thomas M, Smith R T, O’Boyle N M, de Graaf C & Bender A, Comparison of structure-and ligand-based scoring functions for deep generative models: A GPCR case study, *J Cheminform*, **13** (2021) 1–20.
  - 32 Kenny P W, The nature of ligand efficiency, *J Cheminform*, **11** (2019) 1–18.

- 33 de Souza Neto L R, Moreira-Filho J T, Neves B J, Maidana R L B R, Guimarães A C R, Furnham N, Andrade C H & Silva Jr F P, *In silico* strategies to support fragment-to-lead optimization in drug discovery, *Front Chem*, **8** (2020) 93.
- 34 Iqbal M, Javed N, Sahi S T & Cheema N M, Genetic management of bakanae disease of rice and evaluation of various fungicides against *Fusarium moniliforme* *in vitro*, *Pak J Phytopathol*, **23** (2011) 103–107.
- 35 Sunder S Singh R & Dodan D S, Management of bakanae disease of rice caused by *Fusarium moniliforme*, *Indian J Agric Sci*, **84** (2013) 48–52.
- 36 Sunani S K, Bashyal B M, Kharayat B S, Prakash G, Krishnan S G & Aggarwal R, Identification of rice seed infection routes of *Fusarium fujikuroi* inciting bakanae disease of rice, *J Plant Pathol*, **102** (2020) 113–121.
- 37 Aurangzeb M, Ahmed J & Ilyas M B, Chemical control of Bakanae disease of rice caused by *Fusarium moniliforme*, *Pak J Phytopathol*, **10(1)** (1998) 14–7.
- 38 Singh R & Sunder S, Foot rot and bakanae of rice: An overview, *Rev Plant Pathol*, **5** (2012) 565–604.
- 39 Dongmo A N, Nguéfack J, Dongmo J B L, Fouelefack F R, Azah R U, Nkengfack E A & Stefani E, Chemical characterization of an aqueous extract and the essential oil of *Tithonia diversifolia* and their biocontrol activity against seed-borne pathogens of rice, *J Plant Dis Prot*, **128** (2021) 703–713.
- 40 Wan J, Jin Z, Zhong S, Schwarz P, Chen B & Rao J, Clove oil-in-water nanoemulsion: Mitigates growth of *Fusarium graminearum* and trichothecene mycotoxin production during the malting of *Fusarium* infected barley, *Food chem*, **312** (2020) 126120.